Acid-sensing ion channels in mouse olfactory bulb M/T neurons

Ming-Hua Li,[1] Selina Qiuying Liu,[2] Koichi Inoue,[3] Jinquan Lan,[4] Roger P. Simon,[3] and Zhi-Gang Xiong[3]

[1]Department of Neurological Surgery, Oregon Health & Science University, Portland, OR 97239
[2]Oregon State University, Corvallis, OR 97331
[3]Department of Neurobiology, Neuroscience Institute, Morehouse School of Medicine, Atlanta, GA 30310
[4]Legacy Research, Portland, OR 97234

The olfactory bulb contains the first synaptic relay in the olfactory pathway, the sensory system in which odorants are detected enabling these chemical stimuli to be transformed into electrical signals and, ultimately, the perception of odor. Acid-sensing ion channels (ASICs), a family of proton-gated cation channels, are widely expressed in neurons of the central nervous system. However, no direct electrophysiological and pharmacological characterizations of ASICs in olfactory bulb neurons have been described. Using a combination of whole-cell patch-clamp recordings and biochemical and molecular biological analyses, we demonstrated that functional ASICs exist in mouse olfactory bulb mitral/tufted (M/T) neurons and mainly consist of homomeric ASIC1a and heteromeric ASIC1a/2a channels. ASIC activation depolarized cultured M/T neurons and increased their intracellular calcium concentration. Thus, ASIC activation may play an important role in normal olfactory function.

The Journal of General Physiology

INTRODUCTION

The olfactory bulb, which receives input from the primary olfactory fibers of the sensory mucosa, is the first synaptic relay center in the olfactory pathway (Shepherd, 1972). The olfactory bulb is a laminar structure containing two distinct neuronal populations (Mori, 1987). Excitatory projection neurons populate the mitral cell layer, whereas inhibitory interneurons are located in the glomerular layer and granule cell layer. The mitral cells have the largest cell bodies and nuclei in the bulb. Their axons serve as the major outflow from the bulb. The mitral/tufted (M/T) cells in the primary pathway of the olfactory central nervous system (CNS) are thought to be the first signal integrator for extracting odor quality (Imamura et al., 1992).

Ion channels play important roles in odorant detection and normal olfactory function (Vodyanoy and Murphy, 1983; Labarca et al., 1988; Trombley and Shepherd, 1993; Usrey, 2002). Like other excitable cells, both voltage-gated ion channels and ligand-gated channels exist in the membrane of olfactory bulb neurons (Bhalla and Bower, 1993).

Acid-sensing ion channels (ASICs) are ligand-gated channels activated by extracellular protons. They belong to the epithelial sodium channel/degenerin superfamily (Waldmann and Lazdunski, 1998; Krishtal, 2003; Gründer and Chen, 2010). Four genes encoding six ASIC subunits have been identified (Wemmie et al., 2006; Sherwood et al., 2012). Recent analysis of chicken ASIC1a crystal structure showed that ASICs exist as trimers (Jasti et al., 2007). Accumulating evidence has suggested that ASICs play important roles in both physiological and pathological conditions (Price et al., 2000, 2001; Immke and McCleskey, 2001; Johnson et al., 2001; Lin et al., 2002; Wemmie et al., 2002, 2003; Ettaiche et al., 2004; Xiong et al., 2004; Zha et al., 2006; Sherwood and Askwith, 2009; Chu et al., 2011; Pignataro et al., 2011; Sherwood et al., 2012), from sensory transduction to learning/memory, retinal integrity, seizure termination, and ischemia-mediated neuronal injury. However, whether functional ASICs are expressed in the olfactory system and whether they play a role in normal olfactory function are unclear.

Using in situ hybridization, a high level of ASIC1a mRNA has been detected in the olfactory bulb (Bassilana et al., 1997). However, there has been no study characterizing the electrophysiological and pharmacological properties of ASICs in olfactory bulb neurons. Here, we demonstrate that, in both cultured and acutely dissociated M/T neurons, acid stimulation can activate large transient, amiloride-sensitive inward currents. Detailed electrophysiological and pharmacological characterizations suggest that homomeric ASIC1a and heteromeric ASIC1a/2a channels are largely responsible for proton-induced currents in these neurons.

M.-H. Li, S.Q. Liu, and K. Inoue contributed equally to this paper.
Correspondence to Zhi-Gang Xiong: zxiong@msm.edu

Abbreviations used in this paper: ASIC, acid-sensing ion channel; CNS, central nervous system; GABAergic, γ-aminobutyric acid; GAPDH, glyceraldehydes-3-phosphate dehydrogenase; M/T, mitral/tufted; NAAG, dipeptide *N*-acetylaspartylglutamate; PcTX1, psalmotoxin 1; RT, reverse transcription.

The Rockefeller University Press $30.00
J. Gen. Physiol. Vol. 143 No. 6 719–731
www.jgp.org/cgi/doi/10.1085/jgp.201310990

MATERIALS AND METHODS

Ethical approval

The protocol for the use of mice in this paper was reviewed and approved by the Institutional Animal Care and Use Committee.

Primary culture of olfactory bulb neurons

Primary neuronal culture was performed as described previously, with minor modifications (Xiong et al., 2004; Wang et al., 2006). In brief, time-pregnant Swiss mice (at embryonic day 16) were anesthetized with isoflurane followed by cervical dislocation. Brains with olfactory bulbs were removed rapidly from fetuses and placed in Ca^{2+}- and Mg^{2+}-free ice-cold PBS. The bulbs were removed with fine scissors under a dissection microscope and placed in Ca^{2+}/Mg^{2+}-free ice-cold PBS, followed by trituration with fire-polished glass pipettes. Cells were counted and plated in poly-L-ornithine–coated culture dishes at a density of 10^6 cells per 35-mm dish. Neurons were cultured with neurobasal medium supplemented with B27 and maintained at 37°C in a humidified 5% CO_2 atmosphere incubator. Cultures were fed twice a week and used for patch-clamp recordings for ~2–3 wk in culture.

Acute isolation of mouse olfactory bulb neurons

Acute dissociation of mouse olfactory bulb neurons was performed as described previously (Xiong et al., 1999). Adult mice were anaesthetized with halothane followed by cervical dislocation. After surgical removal of the whole brain, olfactory bulb tissues were dissected and incubated in oxygenated extracellular solution (see below) containing 3.5 mg/ml papain for 20–30 min at room temperature. Tissues were then washed three times and incubated in enzyme-free extracellular solution for at least 30 min before mechanical dissociation. For dissociation, small pieces of the olfactory bulb tissues were transferred into a 35-mm culture dish containing 2 ml of extracellular solution (see below). Cells were mechanically dissociated using two fire-polished glass pipettes or fine forceps. Recording began 15 min after the mechanical dissociation.

Electrophysiology

ASIC currents were recorded with the conventional whole-cell patch-clamp technique at room temperature (20–22°C). In general, cells were voltage clamped at −60 mV unless specified otherwise. For rapid changes of extracellular solutions, a multibarrel fast perfusion system (SF-77; Warner Instruments) was used. With this system, complete solution changes are typically achieved within 50 msec. Patch pipettes were pulled from borosilicate glass (1.5-mm diameter; World Precision Instruments) on a two-stage puller (PP83; Narishige). Pipettes had a resistance of 2–4 MOhm when filled with the intracellular solution. Whole-cell patch-clamp recordings were made from large pyramidal-shaped M/T cells with a positive response to dipeptide *N*-acetylaspartylglutamate (NAAG).

During each experiment, a voltage step of −10 mV from the holding potential was applied periodically to monitor cell capacitance and access resistance. Recordings in which access resistance or capacitance changed by >15% during the experiment were excluded for data analysis. In general, ASIC channels were activated by reducing the extracellular pH from 7.4 to specific target levels every 2 min. Data were low-pass filtered at 2 KHz and digitized at 5 KHz.

Solutions

Extracellular solution or fluid (ECF) contained (mM): 140 NaCl, 5.4 KCl, 2 $CaCl_2$, 1 $MgCl_2$, 20 HEPES, and 10 glucose; pH was adjusted to 7.4 or the values indicated, with NaOH/HCl, and the osmolarity was adjusted to 320–330 mOsm. Intracellular solution contained (mM): 140 CsF, 2 TEA-Cl, 5 EGTA, 10 HEPES, 1 $CaCl_2$, and 4 $MgCl_2$, with pH 7.3 adjusted with CsOH/HCl, 290–300 mOsm. For solutions with a pH of <6.0, HEPES was replaced by MES for more reliable pH buffering. To test NAAG response, 10 µM glycine was included in the Mg^{2+}-free extracellular solution. A stock solution of amiloride at 100 mM was prepared in DMSO. The final concentration of DMSO at 0.1% was found to have no effect on the ASIC currents (not depicted). Psalmotoxin 1 (PcTX1) was prepared in distilled water as a stock solution of 20 µM.

Ca^{2+} imaging

Fura-2–based fluorescent Ca^{2+} imaging was performed as described previously (Wang et al., 2006). Olfactory bulb neurons grown on 25-mm glass coverslips were washed three times with ECF and incubated with 5 µM Fura-2-AM for ~40 min at room temperature. Neurons were then washed three times and incubated in normal ECF for 30 min. Coverslips with Fura-2–loaded neurons were transferred to a perfusion chamber on the stage of an inverted microscope (TE300; Nikon). Cells were illuminated using a xenon lamp (75W) and observed with a 40× UV fluor oil-immersion objective lens (both from Nikon). Video images were obtained using a cooled CCD camera (KAF 1401; Sensys; Photometrics). Digitized images were acquired, stored, and analyzed in a PC controlled by Axon Imaging Workbench software (AIW; version 2.1; Axon Instruments). The shutter and filter wheel (Lambda 10-2; Sutter Instrument) were also controlled by AIW to allow timed illumination of cells at 340- and 380-nm excitation wavelengths. Fura-2 fluorescence was detected at an emission wavelength of 510 nm. Ratio images of 340/380 nm were acquired every 500 ms and analyzed by averaging pixel ratio values in circumscribed regions of cells in the field of view. The values were exported from AIW to SigmaPlot (Systat Software) for further analysis and plotting.

Reverse transcription (RT)–PCR

Total RNAs were extracted from olfactory bulb tissues of adult mice with the RNeasy kit (QIAGEN) according to the manufacturer's instructions. cDNAs were then synthesized from 0.2 µg of total RNA in 20-µl volume by RT using oligo $(dT)_{15}$ and Superscript II (Invitrogen) according to the manufacturer's protocol. The sequences of primers used in this study are described as follows: ASIC1a, forward: 5′-ATGGAACTGAAGACCGAGGAGGAG-3′, reverse: 5′-CGCTGCAGGCCTCCCCTCGGAAGT-3′; ASIC1b, forward: 5′-GGCCTTTGTCATAGCACTGGGTGC-3′, reverse: 5′-TTCCCATACCGCGTGAAGACCAC-3′; ASIC2a, forward: 5′-CGCCAACACCTCTACTCTCC-3′, reverse: 5′-TGCCATCCTCGCCTGAGTTA-3′; ASIC2b, forward: 5′-CCTTGGCTTGCTGTTGTCCT-3′, reverse: 5′-TGCCATCCTCGCCTGAGTTA-3′; ASIC3, forward: 5′-GTCTGGACCCTGCTGAACAT-3′, reverse: 5′-GGCTCTGGATCAAAGTCGGG-3′; glyceraldehydes-3-phosphate dehydrogenase (GAPDH), forward: 5′-ATGCTGGTGCTGAGTATGTCGTG-3′, reverse: 5′-TTACTCCTTGGAGGCCATGTAGG-3′. GAPDH was used as the endogenous control. PCR reactions were performed using 0.25 µl of cDNAs as templates in 1× PCR reaction buffer, 0.2 mM each of dNTP, 0.2 ml DNA polymerase mix (AdvantageTM cDNA Polymerase Mix; BD), and 333 nM each of primer in 10 µl of reaction volume. The PCR amplification consisted of denaturation at 94°C for 3 min, 27 cycles of denaturation at 94°C for 30 s, annealing at 61°C for 15 s, and extension at 72°C for 30 s. For a part of Fig. 6 B, multiplex RT-PCR was performed in which primer pairs of each ASIC subunit and GAPDH were added in a reaction. PCR products were separated by electrophoresis on a 1.5% agarose gel, detected using ethidium bromide, and sequenced.

Western blotting

Western blot analysis of ASICs was performed as described in our previous studies (Chai et al., 2010). Adult mouse olfactory bulb tissue was homogenized in ice-cold 1× PBS with a complete protease inhibitor cocktail. Homogenate was mixed with the same volume of 1× PBS containing protease inhibitor cocktail and 2% Triton X-100. The resulting homogenate in 1% Triton X-100/PBS was then incubated with gentle rocking or rotating at 4°C for 30 min. This was followed by centrifugation at 10,000 rpm for 10 min at 4°C. The supernatant (lysates) was collected in a new tube. The total protein concentration of the lysates was measured. The protein samples were mixed with an equal volume of 8 M urea and 5× loading buffer (1/4 volume of sample and urea mixture). The resulting solution was then heated at 95°C for 5 min. Samples were loaded in SDS-PAGE gel (10% gel with 1.5-mm width) and run at 150 V. Protein samples were separated by SDS-PAGE and transferred to polyvinylidene difluoride membranes. The membranes were blocked in PBS containing 5% milk (blocking buffer) and probed with primary antibody diluted in blocking buffer (1:1,000; rabbit anti–rat ASIC1a; Sigma-Aldrich; 1:500; rabbit anti–rat ASIC2a; Alpha Diagnostics Intl. Inc.; and 1:2,000; rabbit anti-actin; Sigma-Aldrich) for 2 h. After an extensive wash with PBS, membranes were probed with horseradish peroxidase–conjugated secondary antibodies (1:1,000; Cell Signaling) and an enhanced luminescence kit (GE Healthcare). Horseradish peroxidase–bound immunoblot was visualized with enhanced chemiluminescence (GE Healthcare) and film (BioMax Chemiluminescence; Kodak).

Immunohistochemical study

Adult WT ASIC1 knockout (ASIC1−/−) and ASIC2 knockout (ASIC2−/−) mice (provided by M. Welsh, J. Wemmie, and M. Price, University of Iowa, Iowa City, IA; Price et al., 2000; Wemmie et al., 2002) with a C57BL/6 background were deeply anesthetized with isoflurane, and the brains with olfactory bulbs were rapidly removed and immediately frozen with dry ice. Frozen olfactory bulb horizontal slices (12 µm) were cut on a cryostat and fixed with 3% formalin and permeabilized with 3% Triton X-100. The slices were then blocked with PBS containing 2% BSA and 2% goat serum for 20 min, followed by incubation overnight at 4°C with primary antibodies against ASIC1a (1:50; SAB2104215; Sigma-Aldrich), ASIC2a (1:50; EDEG11A; Alpha Diagnostics Intl. Inc.), and NeuN (1:350; MAB377; EMD Millipore). Detection was done using secondary antibodies FITC-goat anti–rabbit (1:700) and Cy3 goat anti–mouse (1:350). The specificity of anti-ASIC1a and ASIC2a antibodies was confirmed by immunolabeling of ASIC1a- and ASIC2a-transfected Chinese hamster ovary cells (not depicted). Omitting primary antibodies served as negative control.

Fluorescence images were acquired using Axioskop 2 plus (Carl Zeiss) equipped with AxioCam HRc (Carl Zeiss). All settings used were identical for comparative images. Digital images were equally adjusted in Adobe Photoshop (version 6.0; Adobe) for contrast, brightness, and merging. The color balance was not altered.

Data analysis

Electrophysiology data were acquired using an amplifier (Axopatch 200B; Molecular Devices) with software (pClamp 8.1; Molecular Devices). Data were analyzed using Clampfit (Molecular Devices). The pH_{50} values for H^+ dose–response and steady-state inactivation curves were fitted using the following equation (Wang et al., 2006): $I = \alpha/(1 + (C_{50}/pH)^n)$, where α is the normalized amplitude of the ASIC current, C_{50} is the pH at which a half-maximal response occurs, and n is the Hill coefficient. Time constant of desensitization (τ) and recovery from desensitization were determined using a mono-exponential fit.

Results were expressed as the mean ± SEM. Student's *t* test and one-way ANOVA were used where appropriate to examine the statistical significance of the data. The criterion for significance was set at $P < 0.05$.

Online supplemental material

Fig. S1 shows a histogram plot of PcTX1 inhibition of the ASIC current in cultured olfactory bulb neurons. The online supplemental material is available at http://www.jgp.org/cgi/content/full/jgp.201310990/DC1.

RESULTS

Identification of M/T neurons in culture

Previous studies by Trombley and Westbrook (1990) have shown that primary cultured olfactory bulb neurons can be divided into two major morphologically distinct populations: large pyramidal-shaped neurons (soma diameter of 20–40 µm) and small bipolar neurons (soma diameter of 5–10 µm). Stimulation of the large pyramidal-shaped neurons evokes excitatory postsynaptic potentials, suggesting that they are excitatory glutamatergic neurons (Trombley and Westbrook, 1990). These neurons include M/T cells, which are immunoreactive to NAAG. The small bipolar neurons are γ-aminobutyric acid (GABAergic) interneurons. Stimulating these neurons induces inhibitory postsynaptic potentials. They include most of the granule cells (Trombley and Westbrook, 1990).

Similar to the report by the previous studies, two major groups of neurons can be identified in our culture conditions (Fig. 1 A). To further verify the phenotype of the neurons in our culture conditions, we performed immunocytochemical staining with antibodies against glutaminase (for glutamatergic neurons) and glutamic acid decarboxylase (for GABAergic neurons), as well as neuronal marker (NeuN). Consistent with the previous finding (Trombley and Westbrook, 1990), both glutaminase (large neurons) and glutamic acid decarboxylase immunoactivity (smaller neurons) were detected in our culture conditions (not depicted).

In this study, we focused on M/T cells based on their large size (soma diameter of ∼20–40 µm), pyramidal shape, and positive response to 100 µM NAAG (Neale et al., 2000; Shors et al., 2001). To exclude potential glia cell contamination, Na^+ current was also recorded from each cell. Only large pyramidal cells with Na^+ current and NAAG-induced current were included in the data analysis (Fig. 1, B and C).

Acid-activated currents in M/T neurons

In 155 out of 160 large pyramidal M/T neurons tested, rapid drop of the extracellular pH from 7.4 to 6.0, at a holding potential of −60 mV, evoked large (>500 pA) transient inward currents (Fig. 1 D). In 5 out of the 160 cells, <15 pA acid-evoked currents were recorded (not depicted). For these neurons, no further studies were performed. The current–voltage plot in the majority of large pyramidal M/T neurons showed a linear relationship with a reversal potential close to Na^+ equilibrium

potential (approximately +50 mV; Fig. 1 E). The acid-evoked current was largely inhibited by 100 μM amiloride, a nonspecific blocker for ASICs, with an IC_{50} of 10.92 ± 2.43 (n = 7; Fig. 1 F). Collectively, these data indicate that M/T neurons in the olfactory bulb express functional ASICs.

In mouse cortical and hippocampal neurons, ASIC1a-containing channels such as homomeric ASIC1a, heteromeric ASIC1a/ASIC2a, and ASIC1a/2b channels are largely responsible for acid-activated currents (Baron et al., 2002; Askwith et al., 2004; Chu et al., 2004; Sherwood et al., 2011). To determine the contribution of individual ASIC subunits to acid-activated current in olfactory bulb M/T neurons, we studied the ASIC current in M/T neurons cultured from ASIC1−/− and ASIC2−/− mice (Price et al., 2000; Wemmie et al., 2002). As for ASIC1 knockout mice, exons encoding the first 1–121 amino acids of ASIC1a were withdrawn (Wemmie et al., 2002). For ASIC2 knockout mice, exons encoding the second transmembrane domain were removed, resulting in the lack of both ASIC2a and ASIC2b (Price et al., 2000). In all neurons cultured from ASIC2−/− mice, large ASIC currents (>500 pA) were recorded (Fig. 1 G; n = 20). In these neurons, the decay for the acid-activated current appears to be slower than the current recorded in neurons from the WT mice (2.28 ± 0.28 s vs. 1.16 ± 0.10 s; n = 9 and 49; $P < 0.01$; Fig. 1 G). 10 nM PcTX1, an inhibitor for homomeric ASIC1a and heteromeric ASIC1a/2b channels, largely inhibited the acid-activated current, suggesting that almost all neurons express either homomeric ASIC1a or heteromeric ASIC1a/2b channels (Fig. 1 G). In contrast, in all neurons cultured from the ASIC1−/− mice, no current was activated with a pH drop to as low as 4.0, although a large NMDA current was readily recorded (n = 38; Fig. 1 H). Because ASIC1a subunit is known to be essential for the amplitude of acid-activated current whereas ASIC2 likely affects the desensitization of the current (Askwith et al., 2004), our findings suggest that both ASIC1a and ASIC2 likely contribute to the ASIC

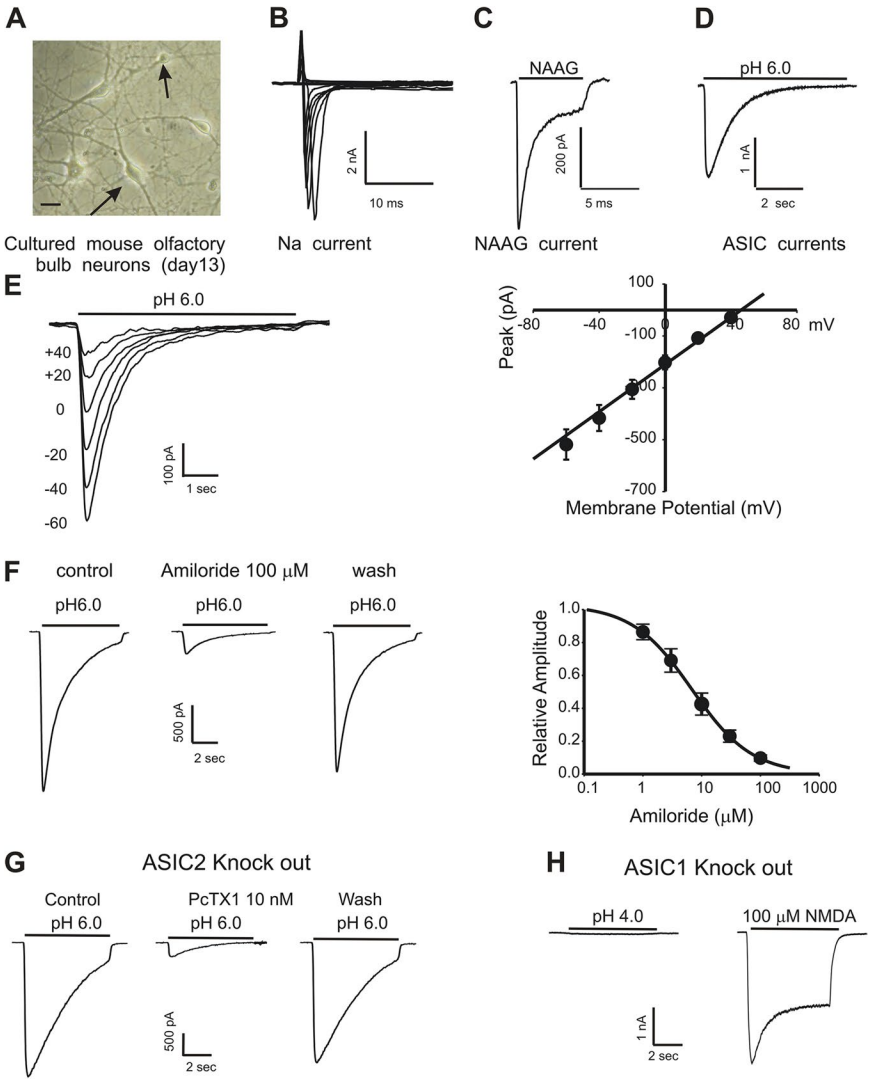

Figure 1. Characterization of ASIC currents in cultured olfactory bulb neurons. (A) Image of olfactory bulb neurons. top and bottom arrows indicate typical small bipolar and large pyramidal-shaped neurons, respectively. (B) Tetrodotoxin-sensitive Na^+ current. (C) NAAG-induced current. (D) ASIC currents in cultured olfactory bulb neurons. (E) Representative traces and summary data demonstrating the current–voltage relationship in cultured olfactory bulb M/T neurons. The acid-activated currents in cultured olfactory bulb M/T neurons have a near linear current–voltage relationship with a reversal potential at approximately +60 mV (n = 5). (F) Dose-dependent blockade of ASIC currents by amiloride. IC_{50} = 10.92 ± 2.43 μM. (G) ASIC current recorded in cultured olfactory bulb M/T neurons from ASIC2−/− mice was significantly inhibited by 10 nM PcTX1. (H) No ASIC current was recorded in cultured M/T neurons from ASIC1−/− mice, where normal NMDA current was recorded. Bar, 40 μm.

currents in M/T neurons. The lack of acid-activated current in ASIC1−/− neurons may suggest that mouse olfactory bulb M/T neurons do not express homomeric ASIC2a (and heteromeric ASIC2a/2b) channels.

Detailed electrophysiological properties of ASICs in M/T neurons

ASIC currents mediated by different configurations of ASIC subunits show distinct pH sensitivity and kinetic properties (Wemmie et al., 2006). For example, homomeric ASIC1a or heteromeric ASIC1a/ASIC2a channels have higher sensitivity to H^+ with a pH_{50} of ~6.2 (Waldmann et al., 1997b; Gründer and Chen, 2010), whereas homomeric ASIC2a channels have the lowest sensitivity to H^+ with a pH_{50} of ~4.4 (Waldmann et al., 1999; Hesselager et al., 2004). In addition, homomeric ASIC1a or heteromeric ASIC1a/ASIC2a channels show faster desensitization, whereas homomeric ASIC2 channels do not. To determine the potential configurations of ASICs in large pyramidal M/T neurons, we first determined pH-dependent activation of the ASIC current in these neurons. As shown in Fig. 2 A, the amplitude of ASIC currents increased with decreasing extracellular pH. The half-maximum activation of ASICs (pH_{50}) is 6.02 ± 0.12, with a Hill coefficient of 1.17 ± 0.14 (n = 10; Fig. 2 B). This pH_{50} value is close to the ASIC currents mediated by homomeric ASIC1a and/or heteromeric ASIC1a/ASIC2a channels (Chu et al., 2004). Because pH sensitivity of homomeric ASIC1a and heteromeric ASIC1a/ASIC2a channels is similar, it is technically difficult to separate them by pH dose–response fitting.

Next, we studied the steady-state inactivation of ASICs in M/T neurons as described previously (Wang et al., 2006; Sherwood and Askwith, 2009). Neurons were incubated in extracellular solutions at various conditioning pH values between 8.0 and 6.5 for ~4 min before the currents were activated by a drop in pH to 5.0. The amplitude of the current activated with different conditioning pH values was normalized to the one activated with a conditioning pH of 8.0 (where there is no apparent

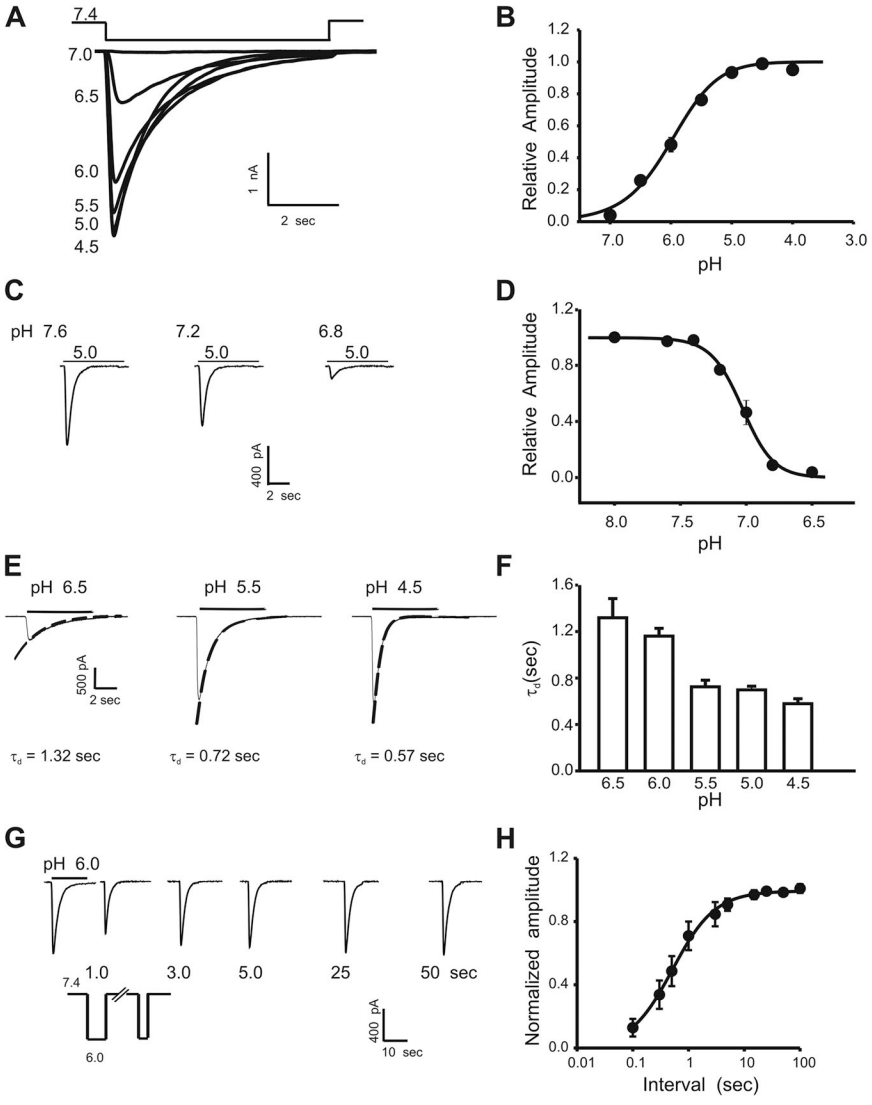

Figure 2. Electrophysiology of ASICs in cultured olfactory bulb M/T neurons. (A and B) Representative traces and summary data showing the pH dependence of ASIC currents activated by pH drop from 7.4 to values indicated. Dose–response curves were fitted to the Hill equation with an average pH_{50} of 6.02 ± 0.12 (n = 10). (C and D) Representative traces and summary data showing steady-state inactivation of ASIC currents in mouse olfactory bulb M/T neurons. The half-maximum inactivation of ASIC current was 7.08 ± 0.10 (n = 10). (E and F) Representative currents and summary data showing pH-dependent desensitization of the ASIC currents in olfactory bulb M/T neurons. The time constants of desensitization (τ_{des}) were 1.32 ± 0.06 s, 1.16 ± 0.07 s, 0.72 ± 0.06 s, 0.69 ± 0.03 s, and 0.57 ± 0.04 s at pH 6.5, 6.0, 5.5, 4.5, and 4.0, respectively. (G) Example current traces showing time-dependent recovery of ASIC currents from desensitization in olfactory bulb neurons. (H) Summary graph showing the recovery rate of ASIC current from desensitization in mice olfactory bulb M/T neurons. The recovery time constant (τ_{rec}) was 1.08 ± 0.50 s. Each plotted point represents the average ± SEM of data from 10 cells; each cell was stimulated at all the time points.

inactivation) and plotted against the value of conditioning pH. As shown in Fig. 2 C, the amplitude of the ASIC current decreases with decreasing conditioning pH. Plot of the steady-state inactivation curve revealed a pH for half-maximum inactivation (pH_{50}) at 7.08 ± 0.10 (Fig. 2 D; n = 10).

Next, we investigated the desensitization properties of ASIC currents in large M/T neurons. The desensitization rate was measured by fitting the decay phase of the current with a single-exponential function (Xiong et al., 2004; Wang et al., 2006). The decay time constant (τ_d) for ASIC currents activated at pH 6.0 was 1.16 ± 0.07 s (n = 65), which is slightly faster than the decay time constant for ASIC currents in mouse cortical neurons (1.79 ± 0.11 s; n = 33; P < 0.01; Li et al., 2010). Consistent with previous reports for ASIC currents mediated by ASIC1a-containing channels (Hesselager et al., 2004; Li et al., 2010), the desensitization rate of the ASIC current in M/T neurons is pH dependent. At pH 6.5, 5.5, 4.5, and 4.0, the decay time constant (τ_d) was 1.32 ± 0.06 s, 0.72 ± 0.06 s, 0.69 ± 0.03 s, and 0.57 ± 0.04 s, respectively (n = 5–6; Fig. 2, E and F).

The recovery rate of ASICs from desensitization was also studied in large M/T neurons. Currents were activated consecutively by pairs of low pH pulses (from 7.4 to 6.0), with various time intervals (e.g., 0.5, 1, 3, 5, 15, 25, and 50 s) between the end of the first and the beginning of the second acid exposure. The peak amplitude of the second current was then normalized to the first one and plotted against the time intervals between the two acid exposures. The recovery rate of ASIC currents from desensitization in M/T neurons was 1.08 ± 0.50 s (n = 10; Fig. 2, G and H), which is close to that recorded in mouse cortical neurons (Wang et al., 2006).

Pharmacological properties of ASIC currents in M/T neurons

In addition to the differences in electrophysiological properties, ASIC currents mediated by different ASIC configurations or subunits have distinct pharmacological profiles (Xiong et al., 2007; Chu et al., 2011). Although all ASICs are sensitive to the blockade by amiloride, only homomeric ASIC1a channels and heteromeric ASIC1a/2b channels are inhibited by PcTX1 (Escoubas et al., 2000; Sherwood et al., 2011). Although low nanomolar concentrations of Zn^{2+} inhibit ASIC1a-containing channels (Chu et al., 2004), high micromolar concentrations of Zn^{2+} (100–300 µM) selectively potentiate the activities of ASIC2a-containing channels (Baron et al., 2001).

To determine the pharmacological properties of ASIC currents in M/T neurons, we studied the sensitivity of ASIC currents to PcTX1 inhibition and Zn^{2+} potentiation. In the presence of 10 nM PcTX1, a near saturating concentration for inhibiting the homomeric ASIC1a channels (Escoubas et al., 2000), the amplitude of ASIC currents was reduced to 60.29 ± 4.76% of the control value in a total of 46 neurons tested (Fig. 3 B, All). This finding suggests that the homomeric ASIC1a or heteromeric ASIC1a/ASIC2b channels are the predominant ASIC configurations in these neurons. We also generated a histogram plot with data from PcTX1 inhibition

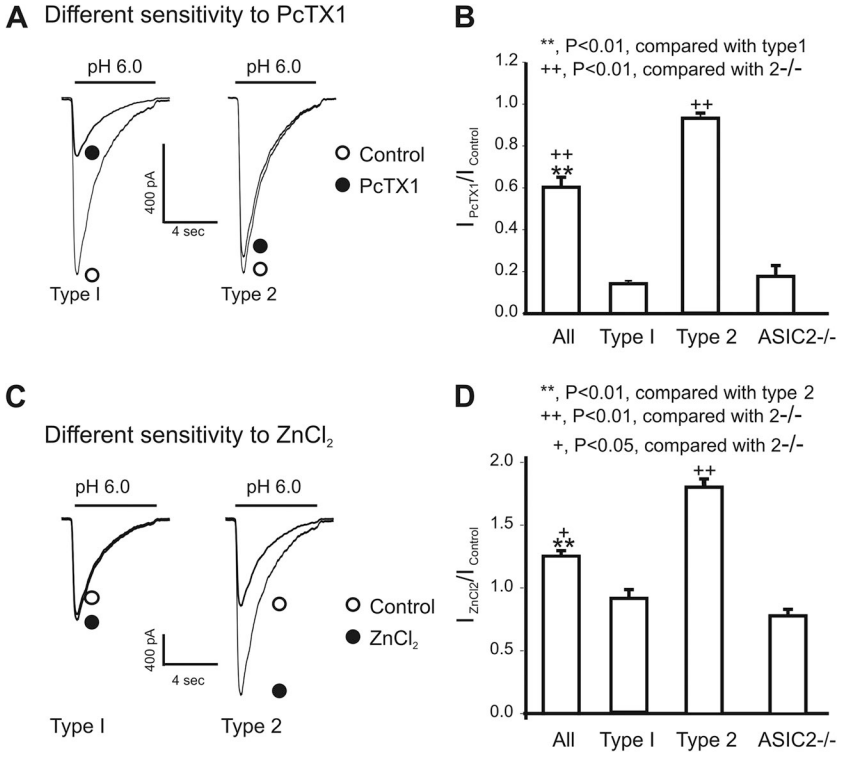

Figure 3. Pharmacological properties of ASIC currents in mouse olfactory bulb M/T neurons. (A and B) Representative traces and summary data showing different responses of ASIC currents in M/T neurons to 10 nM PcTX1. Significant inhibition of the ASIC current by PcTX1 was seen in type 1 neurons compared with type 2 neurons, where small inhibition was seen. **, P < 0.01 compared with type 1; ++, P < 0.01 compared with 2−/−. (C and D) Representative current traces and summary data showing different sensitivity of ASIC currents to zinc potentiation in type 1 and type 2 neurons. The potentiation of ASIC currents by 200 µM zinc in type 2 neurons was significantly greater compared with type 1 neurons. **, P < 0.01 compared with type 2; ++, P < 0.01 compared with 2−/−; +, P < 0.05 compared with 2−/−.

of the ASIC current (Fig. S1). The histogram does show a trend of two major categories corresponding to type 1 (PcTX1/control: 0.1–0.2) and type 2 cells (PcTX1/control: 0.8–0.9). A high concentration of $ZnCl_2$ (200 µM), which potentiates only the ASIC2a-containing channels (Baron et al., 2001), increased the amplitude of ASIC currents by an average of 43.16 ± 8.82% (n = 46; Fig. 3 D, All), supporting the existence of heteromeric ASIC1a/ASIC2a channels.

According to different sensitivity of the ASIC currents to PcTX1 inhibition and Zn^{2+} potentiation, M/T neurons may be divided into two major subpopulations. In 21.74% (10 out of 46) of the M/T neurons, ASIC currents were highly inhibited by 10 nM PcTX1. The amplitude of the current in these neurons was inhibited by 85.78 ± 1.40% (Fig. 3, A and B), which is similar to the results obtained in neurons from ASIC2−/− mice (n = 4). In these neurons, no potentiation of the ASIC current was observed by 200 µM $ZnCl_2$ (Fig. 3, C and D). These neurons were defined as type 1. The acid-activated currents in these neurons are likely mediated predominantly by homomeric ASIC1a or heteromeric ASIC1a/ASIC2b channels. In 54.35% of M/T neurons (25 out of 46), the ASIC currents had little sensitivity to 10 nM PcTX1 (Fig. 3, A and B). However, the currents in these neurons were highly sensitive to $ZnCl_2$ potentiation; the amplitude of the ASIC currents was increased to 1.89 ± 0.20 of the control value in the presence of 200 µM $ZnCl_2$ (Fig. 3, C and D). We defined these neurons as type 2. The currents in type 2 neurons are likely mediated predominantly by the heteromeric ASIC1a/2a channels (Baron et al., 2001). The remaining 23.91% of M/T neurons were inconsistent in regard to PcTX1 inhibition and Zn^{2+} potentiation. The currents were partially inhibited by 10 nM PcTX1 and partially potentiated by 200 µM Zn^{2+}, suggesting a mix of homomeric ASIC1a and heteromeric ASIC1a/ASIC2a channels.

Properties of ASIC currents in acutely dissociated neurons

To gain more information about the properties of ASICs in mature olfactory bulb neurons, neurons were acutely dissociated from the olfactory bulb of adult mice and studied with whole-cell patch-clamp recording. Similar to the cultured neurons, large currents were elicited by dropping the extracellular pH from 7.4 to 6.0 with rapid desensitization (Fig. 4, A–C). Key findings, e.g., inhibition

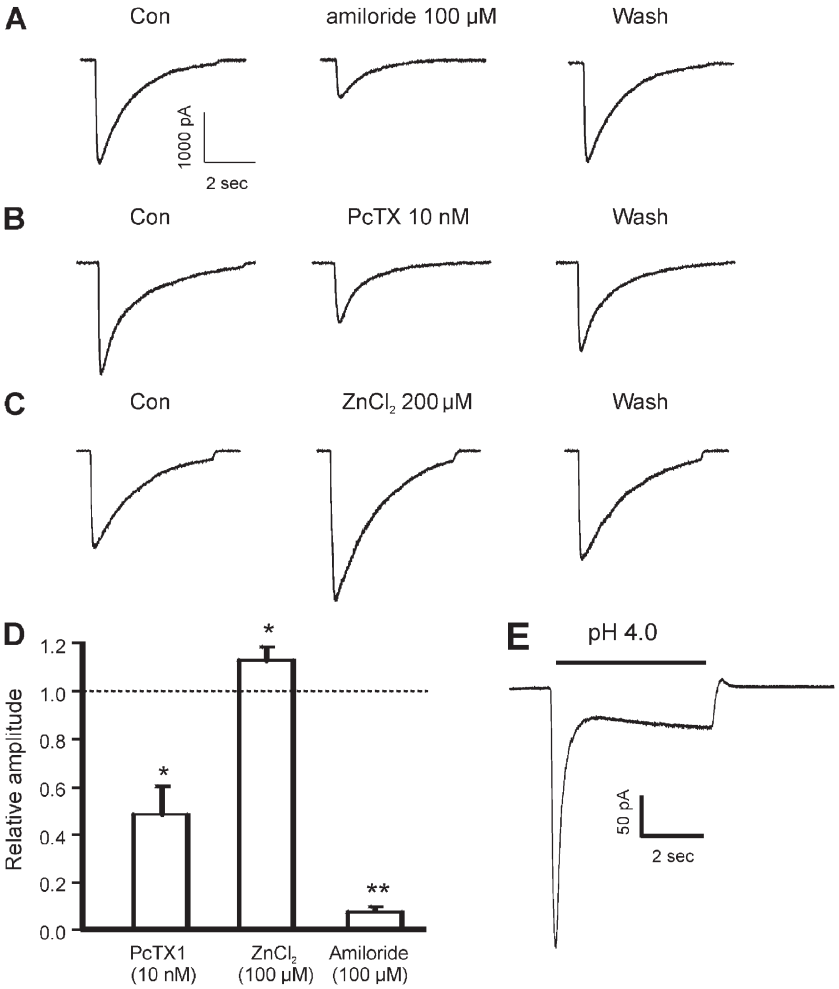

Figure 4. Fundamental properties of ASIC currents in acutely dissociated mouse olfactory bulb M/T neurons. (A) Representative traces showing the ASIC current activated by an extracellular pH drop from 7.4 to 6.0 in the absence and presence of 100 µM amiloride. (B) Representative traces showing the ASIC current activated by an extracellular pH drop from 7.4 to 6.0 in the absence and presence of 10 nM PcTX1. (C) Representative traces showing the ASIC current activated by an extracellular pH drop from 7.4 to 6.0 in the absence and presence of 200 µM $ZnCl_2$. (D) Summary data showing the relative amplitude of acid-activated currents with a pH drop from 7.4 to 6.0 in the presence of indicated agents (n = 3–6). Each cell was subjected to one treatment, and the relative amplitude was derived from the amplitude of the current in the presence of the individual agent divided by its own control value before the treatment. *, $P < 0.05$ compared with control; **, $P < 0.01$ compared with control. (E) Example trace of ASIC current activated by an extracellular pH drop from 7.4 to 4.0. The current shows a slow and sustained component indicative of ASIC3 current.

of the ASIC currents by amiloride and PcTX1, and potentiation by Zn^{2+} were confirmed in acutely dissociated olfactory bulb neurons (Fig. 4, A–D).

We also assessed potential contribution of the ASIC3 subunit to ASIC currents in acutely dissociated neurons. In this regard, we studied the ASIC currents with a pH drop from 7.4 to 4.0. It has been well documented that, at low pH levels such as 5.0 or 4.0, currents carried by ASIC3 (DRASIC) channels show distinct biphasic kinetics: a fast transient current followed by a slow sustained component (Waldmann et al., 1997a). Consistent with the presence of the ASIC3 subunit, a clear biphasic current was recorded in one third of the acutely dissociated olfactory bulb neurons isolated from mature adult mice (Fig. 4 E). In contrast, this slow and sustained current was not visible in the embryonic culture of olfactory bulb neurons (Fig. 2 A). These findings are consistent with the PCR data showing that ASIC3 expression is detected in adult olfactory tissue but not in embryonic culture of olfactory bulb neurons (see below).

ASIC activation mediates neuronal depolarization in M/T neurons

Next, we determined whether activation of ASICs can induce membrane depolarization in M/T neurons. Current clamp recording was used in the presence of blockers of voltage-gated Ca^{2+} channels (5 μM nimodipine) and glutamate receptors (10 μM MK-801 and 20 μM CNQX). As shown in Fig. 5 A, a drop in the extracellular pH from 7.4 to 6.5 induced a large membrane depolarization in these neurons. The membrane potential was depolarized from −60.17 ± 0.02 mV to −22.21 ± 2.93 mV

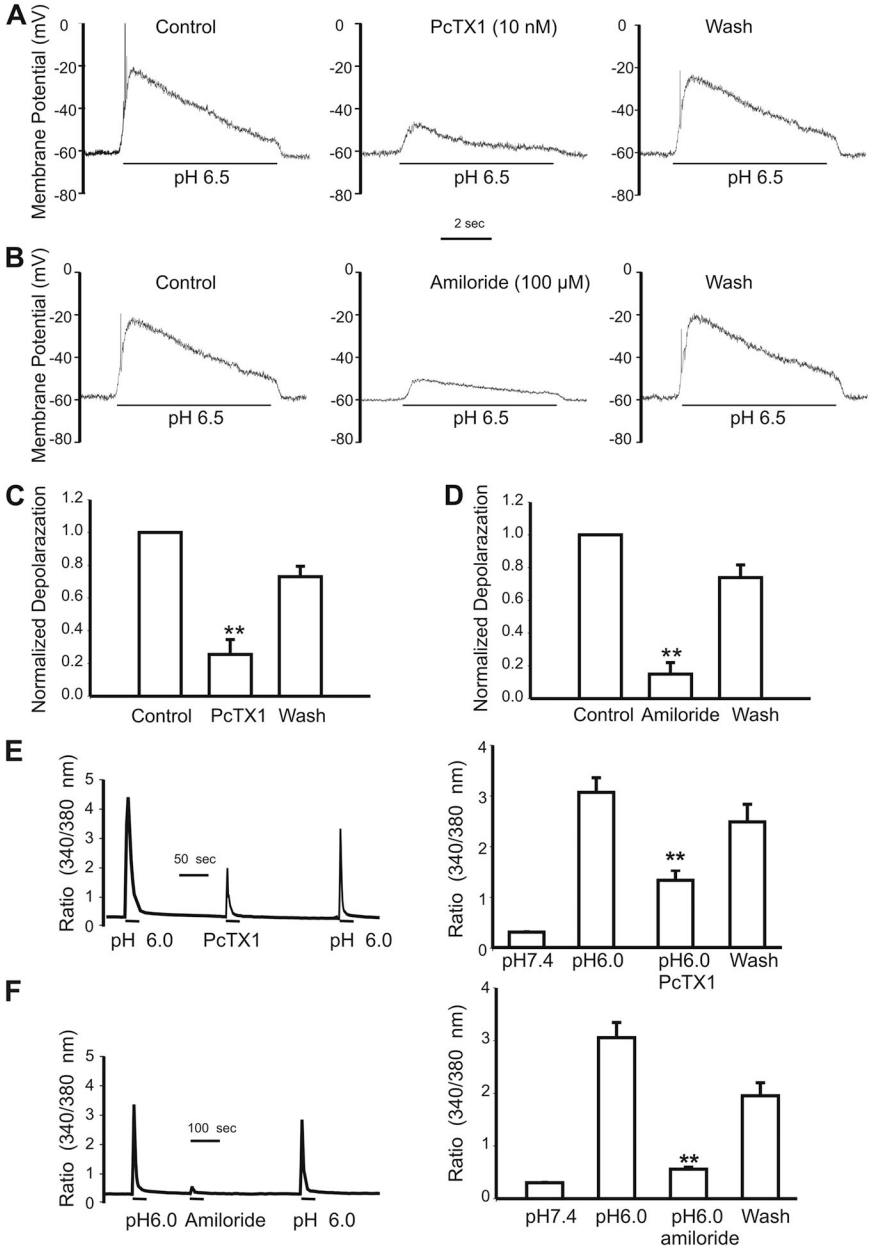

Figure 5. Effects of PcTX1 and amiloride on acid-induced membrane depolarization and intracellular Ca^{2+} increase. (A and B) Representative traces showing membrane depolarization induced by an extracellular pH drop from 7.4 to 6.5 in the presence of 5 μM nimodipine, 10 μM MK-801, and 20 μM CNQX. The acid-induced membrane depolarization in M/T neurons was inhibited by 10 nM PcTX1 and 100 μM amiloride. (C and D) Summary data showing the inhibition of acid-induced membrane depolarization by 10 nM PcTX1 ($n = 8$; **, $P < 0.01$) and 100 μM amiloride ($n = 6$; **, $P < 0.01$). (E) Representative 340/380 ratio and summary data showing increases of intracellular Ca^{2+} ($[Ca^{2+}]_i$) in response to an extracellular pH drop from 7.4 to 6.0, and the inhibition by 10 nM PcTX1. The 340/380 ratio changed from 3.08 ± 0.25 to 1.32 ± 0.18 in the presence of PcTX1 ($n = 10$; **, $P < 0.01$). (F) Representative 340/380 ratio and summary data showing increases of intracellular Ca^{2+} ($[Ca^{2+}]_i$) in response to an extracellular pH drop from 7.4 to 6.0, and the inhibition by 100 μM amiloride. The 340/380 ratio was 0.37 ± 0.05 in the presence of 100 μM amiloride ($n = 8$; **, $P < 0.01$).

in response to a pH drop from 7.4 to 6.5 ($P < 0.01$; $n = 8$). This acid-induced membrane depolarization was attenuated by 10 nM PcTX1 and 100 μM amiloride (Fig. 5, A–D), suggesting that activation of ASICs can produce dramatic membrane depolarization in M/T neurons.

Activation of ASICs in olfactory bulb neurons produces an increase of intracellular Ca^{2+}

An increase of intracellular Ca^{2+} concentration is important for various physiological functions of neurons. To determine if activation of ASICs can produce increases of intracellular Ca^{2+} in M/T neurons, fluorescent Ca^{2+} imaging was performed. The 340/380-nm ratio image was measured in the presence of blockers of glutamate receptors and voltage-gated Ca^{2+} channels (20 μM CNQX, 10 μM MK-801, and 5 μM nimodipine). Similar to mouse cortical neurons (Xiong et al., 2004; Wang et al., 2006), reduction of pH_e from 7.4 to 6.0 induced a large increase of $[Ca^{2+}]_i$ in the majority (>80%) of mouse olfactory bulb neurons independent of the activation of glutamate receptors and voltage-gated Ca^{2+} channels. The ratio of 340/380-nm images increased from 0.42 ± 0.04 to 3.08 ± 0.25 after changing pH_e from 7.4 to 6.0 ($P < 0.01$; $n = 18$). Consistent with the activation of ASIC1a channels, the increase in the 340/380-nm ratio image was inhibited by 10 nM PcTX1 ($P < 0.01$; $n = 10$) and 100 μM amiloride ($P < 0.01$; $n = 8$; Fig. 5, C–F).

Detection of ASIC expression in the mouse olfactory bulb by biochemical/molecular biological analysis

To provide biochemical/molecular biological evidence supporting the existence of ASICs in the mouse

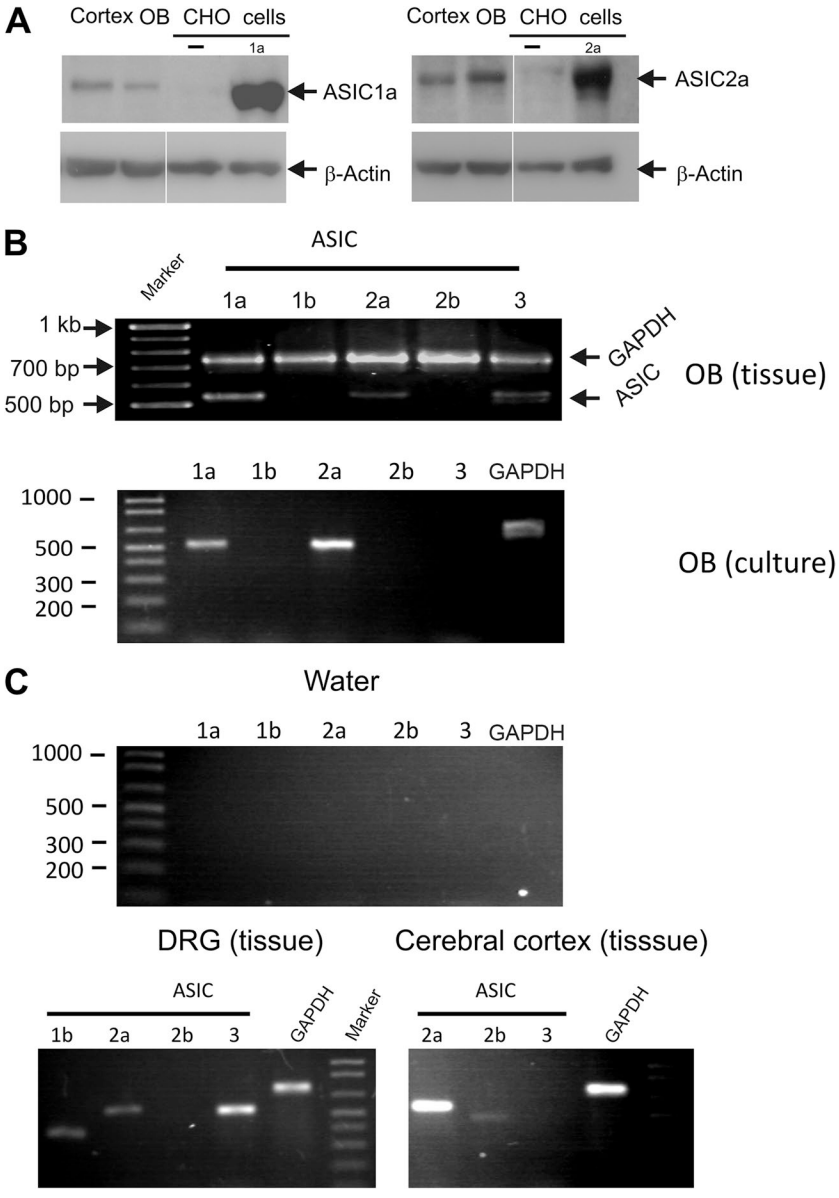

Figure 6. Expression of ASICs in mouse olfactory bulb tissue and cultured neurons detected by Western blot and RT-PCR. (A) Western blot analysis showing the expression of ASIC1a and ASIC2a proteins in mouse olfactory bulb tissue. The data are representative of three independent experiments. White lines indicate that intervening lanes have been spliced out. (B) ASIC1a, ASIC2a, and ASIC3 mRNA were detected in olfactory bulb tissue, whereas ASIC1b and ASIC2b were not (top). ASIC1a and ASIC2a, but not ASIC3, were detectable in mouse olfactory bulb culture (bottom). The data are representative of four (two independent dishes each from two independent cultures) and three (tissue) experiments, respectively. (C) Negative (water) and positive controls for ASIC1b, ASIC2b, and ASIC3 were shown using dorsal root ganglia (for ASIC1b and ASIC3) and cerebral cortex (for ASIC2b). Expected sizes are (in bp) 541 (ASIC1a), 399 (ASIC1b), 548 (ASIC2a), 473 (ASIC2b), 538 (ASIC3), and 723 (GAPDH).

olfactory bulb, we performed Western blot analysis to determine the expression of individual ASIC protein. Adult mouse olfactory bulb tissue was processed and probed with ASIC antibodies as described in Materials and methods. As shown in Fig. 6 A, both ASIC1a and ASIC2a proteins were detected. In addition to ASIC1a and ASIC2a, several studies have suggested the presence of ASIC2b and ASIC3 in CNS neurons (Wu et al., 2004; Baron et al., 2008; Sherwood et al., 2011). Because of the lack of reliable antibodies for these subunits, we performed RT-PCR analysis instead. As shown in Fig. 6 B, ASIC1a and ASIC 2a mRNAs were detected in adult mouse olfactory bulb tissues and in embryonic cultures. However, the expression of ASIC1b and ASIC2b was negligible. Interestingly, ASIC3 was detected in adult olfactory bulb tissue but not in cultured olfactory cells (Fig. 6 B). The discrepancy between adult olfactory tissue and embryonic culture of olfactory bulb cells may suggest a developmental change of the ASIC3 expression in the olfactory bulb. Alternatively, the difference could have been produced by the culture condition.

We next determined the pattern of expression of the ASIC1a and ASIC2a subunit in mouse olfactory bulb slices using immunohistochemical staining. As shown in Fig. 7 A, the laminar structure was seen and most of cells were stained with neuronal marker NeuN. Our results show that both ASIC1a and ASIC2a subunits were expressed by olfactory bulb neurons throughout all laminar structures. The staining of the ASIC1a appears to be expressed in almost every cell and concentrated on the outline of the cell, whereas a large portion of ASIC2a seems to be colocalized with the nucleus (Fig. 7, B, a, and C, a). No immunofluorescence was detected in olfactory bulb slices from ASIC1−/− or ASIC2−/− mice (Fig. 7, B, b, and C, b), indicating the specificity of the staining in the conditions used in this study.

DISCUSSION

Here, we investigated the expression of ASIC subunits in the mouse olfactory bulb and studied the electrophysiological and pharmacological properties of ASICs

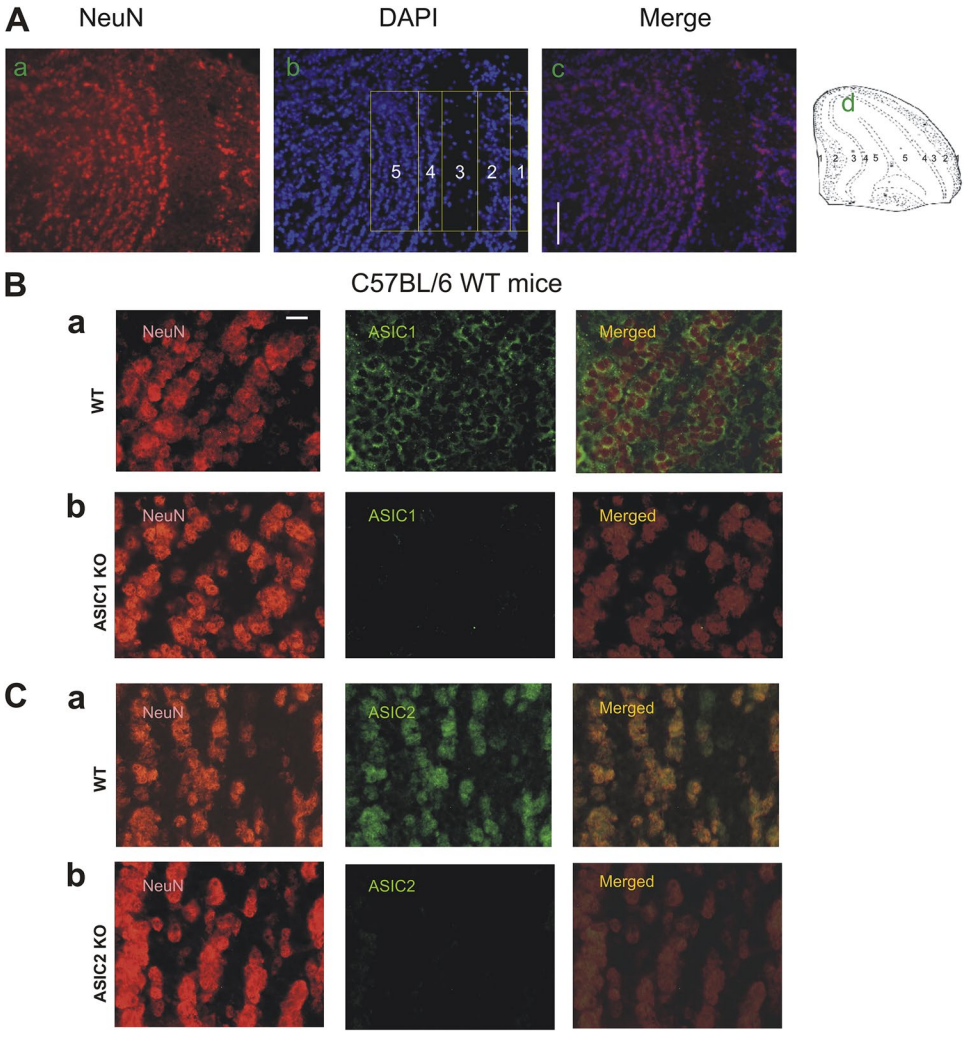

Figure 7. Localization of ASIC1a and ASIC2a protein in WT and ASIC−/− mouse olfactory bulb. (A) Schematic panels show the histological appearance of the olfactory bulb in horizontal sections (a–c) and the corresponding drawing indicating the laminar structure (d). The entire laminar structure is shown with neuronal marker NeuN (a), DAPI (b), and merged (c) images. Bar, 50 µm. (B) Images showing the ASIC1a protein expression in mouse olfactory bulb from WT (Ba) and ASIC1 knockout mice (Bb). (C) Images showing the expression pattern of ASIC2a in mouse olfactory bulb from WT (Ca) and ASIC2 knockout mice (Cb). Based on the overall anatomy of the bulb, the data in B and C are from lamina 5. Bar, 20 µm.

in large pyramidal-shaped M/T neurons using combinations of whole-cell patch-clamp recordings and biochemical/molecular biological techniques.

In almost all large pyramidal-shaped olfactory bulb M/T neurons tested, inward currents with fast activation and desensitization can be induced by drops of extracellular pH below 7.0 (Fig. 1). The acid-induced currents are sensitive to amiloride (IC_{50} of ~10.92 μM), a nonspecific inhibitor of ASICs. The current–voltage plot showed a linear relationship with a reversal potential close to Na^+ equilibrium potential (approximately +50 mV). Collectively, these data support the presence of functional ASICs in these neurons. In addition to Na^+, ASICs in M/T neurons are also permeable to Ca^{2+}. These characteristics of acid-activated currents are similar to the ASIC currents described in mouse cortical neurons (Xiong et al., 2004).

ASICs formed by different subunits have distinct channel kinetics, pH sensitivity, and responses to pharmacological agents. To determine the subunit composition of ASICs in M/T neurons, we characterized the detailed electrophysiological and pharmacological properties of ASICs. For pharmacological characterization, we used PcTX1, which is a specific inhibitor for ASIC1a homomer and ASIC1a/2b heteromer, and $ZnCl_2$, which potentiates the ASIC2a-containing channels at high micromolar concentrations (e.g., >100 μM). Our electrophysiological and pharmacological data suggest that homomeric ASIC1a and heteromeric ASIC1a/2a or ASIC1a/2b channels are likely responsible for the proton-gated currents in the majority of olfactory bulb neurons. Biochemical analyses support the presence of ASIC1a and ASIC2a subunits but not ASIC2b subunits in the olfactory bulb.

The presence of ASIC3 in the brain has been demonstrated in some studies (Babinski et al., 1999; Meng et al., 2009), but the contribution of this subunit to the ASIC current in CNS neurons has never been reported. Our electrophysiological recording results demonstrated that the desensitization of ASICs in cultured cortical neurons is around 1.79 ± 0.12 s (Li et al., 2010), whereas it is 1.16 ± 0.07 s in cultured olfactory bulb neurons. Based on the study by Hesselager et al. (2004), the fast desensitization of the ASIC might indicate the presence of heteromeric ASIC1a/ASIC3 channels. However, this was not supported by the RT-PCR data that show the absence of this subunit in cultured olfactory cells. Therefore, the potential involvement of ASIC3 in the ASIC current of cultured olfactory neurons is not clear. Interestingly, in acutely dissociated mature olfactory bulb neurons, we were able to detect a slow and sustained component of the ASIC current in response to a very low pH (4.0), supporting the presence of the ASIC3 channels (Waldmann et al., 1997a). Whether the difference is caused by developmental change of ASIC3 expression or by the culture condition remains to be determined.

Similar to ASICs in other neurons or neuronal cell lines (Chu et al., 2002; Li et al., 2010), the desensitization rate of ASICs in mouse olfactory bulb M/T neurons is pH dependent, and the greater the decrease in pH the faster the desensitization of the ASIC current. Assuming that synaptic release of protons and activation of ASICs in M/T neurons are involved in olfaction, the feature of faster desensitization in response to stronger stimulation could be a protective mechanism against strong and unpleasant odors.

Contents in synaptic vesicles are highly acidic (Miesenböck et al., 1998). Thus, ASICs are expected to be activated by the release of acidic content of synaptic vesicles and play a role in synaptic transmission (Wemmie et al., 2006). Indeed, studies by Wemmie et al. (2002, 2003) have suggested that activation of ASIC1a channels is involved in synaptic plasticity, learning/memory, and fear conditioning. However, the requirement of ASIC1a for hippocampal learning and memory was not supported by a recent study (Wu et al., 2013). Similar to hippocampus and amygdale, ASIC1a is enriched in the glomerulus of olfactory bulb, an area with strong excitatory synaptic input (Wemmie et al., 2003). However, no direct demonstration of functional ASICs in olfactory bulb neurons and their electrophysiological and pharmacological properties has been provided until now.

Homomeric ASIC1a and heteromeric ASIC1a/ASIC2a channels are the major configurations of ASICs in CNS neurons (Askwith et al., 2004; Chu et al., 2004). Studies in spinal cord neurons by Baron et al. (2008) have suggested that homomeric ASIC1a channel code for low frequency stimulation during sustained extracellular acidification, whereas heteromeric ASIC1a/ASIC2a respond to both low and high frequency stimulations. Based on these findings, it is likely that ASIC1a and ASIC2a channels in olfactory bulb likely coordinate to code for both high and low frequency odorant stimulation.

The olfactory system is also the target of adult neurogenesis (Lledo et al., 2006) and is important for neural plasticity and memory (Linster et al., 2003; Mandairon et al., 2006). Impaired olfactory system was seen in normal (Westenhoefer, 2005; Wilson et al., 2006) and pathological aging subjects (Devanand et al., 2000; Wilson et al., 2007). It has been reported that loss of olfactory perception is one of the first symptoms in Parkinson's disease (Ponsen et al., 2004). It would be interesting to know whether a reduced ASIC expression and/or function are involved in the pathophysiology of this disorder.

The present studies only focused on ASICs in M/T neurons of the olfactory bulb. In addition to M/T cell population, another large population of neurons in olfactory bulb is the GABAergic interneurons. Given the potential difference in the expression profile of ASICs in interneurons as has been shown in hippocampus (Weng et al., 2010), it will be interesting to investigate the presence and electrophysiological/pharmacological

properties of ASICs in GABAergic interneurons of the olfactory bulb in the near future.

We thank Drs. Michael Welsh, John Wemmie, and Margaret Price at University of Iowa for ASIC1−/− and ASIC2−/− mice, and Xiaoming Chen for technical assistance.

The work in Z-.G. Xiong's laboratory is supported in part by National Institutes of Health grants R01NS047506, R01NS066027, U54NS083932, NIMHD S21MD000101, AHA 0840132N, and ALZ IIRG-10-173350.

The authors declare no competing financial interests.

Edward N. Pugh Jr. served as editor.

Submitted: 12 March 2013
Accepted: 17 April 2014

REFERENCES

Askwith, C.C., J.A. Wemmie, M.P. Price, T. Rokhlina, and M.J. Welsh. 2004. Acid-sensing ion channel 2 (ASIC2) modulates ASIC1 H^+-activated currents in hippocampal neurons. *J. Biol. Chem.* 279: 18296–18305. http://dx.doi.org/10.1074/jbc.M312145200

Babinski, K., K.T. Lê, and P. Séguéla. 1999. Molecular cloning and regional distribution of a human proton receptor subunit with biphasic functional properties. *J. Neurochem.* 72:51–57. http://dx.doi.org/10.1046/j.1471-4159.1999.0720051.x

Baron, A., L. Schaefer, E. Lingueglia, G. Champigny, and M. Lazdunski. 2001. Zn^{2+} and H^+ are coactivators of acid-sensing ion channels. *J. Biol. Chem.* 276:35361–35367. http://dx.doi.org/10.1074/jbc.M105208200

Baron, A., R. Waldmann, and M. Lazdunski. 2002. ASIC-like, proton-activated currents in rat hippocampal neurons. *J. Physiol.* 539:485–494. http://dx.doi.org/10.1113/jphysiol.2001.014837

Baron, A., N. Voilley, M. Lazdunski, and E. Lingueglia. 2008. Acid sensing ion channels in dorsal spinal cord neurons. *J. Neurosci.* 28:1498–1508. http://dx.doi.org/10.1523/JNEUROSCI.4975-07.2008

Bassilana, F., G. Champigny, R. Waldmann, J.R. de Weille, C. Heurteaux, and M. Lazdunski. 1997. The acid-sensitive ionic channel subunit ASIC and the mammalian degenerin MDEG form a heteromultimeric H^+-gated Na^+ channel with novel properties. *J. Biol. Chem.* 272:28819–28822. http://dx.doi.org/10.1074/jbc.272.46.28819

Bhalla, U.S., and J.M. Bower. 1993. Exploring parameter space in detailed single neuron models: simulations of the mitral and granule cells of the olfactory bulb. *J. Neurophysiol.* 69:1948–1965.

Chai, S., M. Li, D. Branigan, Z.G. Xiong, and R.P. Simon. 2010. Activation of acid-sensing ion channel 1a (ASIC1a) by surface trafficking. *J. Biol. Chem.* 285:13002–13011. http://dx.doi.org/10.1074/jbc.M109.086041

Chu, X.P., J. Miesch, M. Johnson, L. Root, X.M. Zhu, D. Chen, R.P. Simon, and Z.G. Xiong. 2002. Proton-gated channels in PC12 cells. *J. Neurophysiol.* 87:2555–2561.

Chu, X.P., J.A. Wemmie, W.Z. Wang, X.M. Zhu, J.A. Saugstad, M.P. Price, R.P. Simon, and Z.G. Xiong. 2004. Subunit-dependent high-affinity zinc inhibition of acid-sensing ion channels. *J. Neurosci.* 24:8678–8689. http://dx.doi.org/10.1523/JNEUROSCI.2844-04.2004

Chu, X.P., C.J. Papasian, J.Q. Wang, and Z.G. Xiong. 2011. Modulation of acid-sensing ion channels: molecular mechanisms and therapeutic potential. *Int. J. Physiol. Pathophysiol. Pharmacol.* 3:288–309.

Devanand, D.P., K.S. Michaels-Marston, X. Liu, G.H. Pelton, M. Padilla, K. Marder, K. Bell, Y. Stern, and R. Mayeux. 2000. Olfactory deficits in patients with mild cognitive impairment predict Alzheimer's disease at follow-up. *Am. J. Psychiatry.* 157:1399–1405. http://dx.doi.org/10.1176/appi.ajp.157.9.1399

Escoubas, P., J.R. De Weille, A. Lecoq, S. Diochot, R. Waldmann, G. Champigny, D. Moinier, A. Ménez, and M. Lazdunski. 2000. Isolation of a tarantula toxin specific for a class of proton-gated Na^+ channels. *J. Biol. Chem.* 275:25116–25121. http://dx.doi.org/10.1074/jbc.M003643200

Ettaiche, M., N. Guy, P. Hofman, M. Lazdunski, and R. Waldmann. 2004. Acid-sensing ion channel 2 is important for retinal function and protects against light-induced retinal degeneration. *J. Neurosci.* 24:1005–1012. http://dx.doi.org/10.1523/JNEUROSCI.4698-03.2004

Gründer, S., and X. Chen. 2010. Structure, function, and pharmacology of acid-sensing ion channels (ASICs): focus on ASIC1a. *Int. J. Physiol. Pathophysiol. Pharmacol.* 2:73–94.

Hesselager, M., D.B. Timmermann, and P.K. Ahring. 2004. pH Dependency and desensitization kinetics of heterologously expressed combinations of acid-sensing ion channel subunits. *J. Biol. Chem.* 279:11006–11015. http://dx.doi.org/10.1074/jbc.M313507200

Imamura, K., N. Mataga, and K. Mori. 1992. Coding of odor molecules by mitral/tufted cells in rabbit olfactory bulb. I. Aliphatic compounds. *J. Neurophysiol.* 68:1986–2002.

Immke, D.C., and E.W. McCleskey. 2001. Lactate enhances the acid-sensing Na^+ channel on ischemia-sensing neurons. *Nat. Neurosci.* 4:869–870. http://dx.doi.org/10.1038/nn0901-869

Jasti, J., H. Furukawa, E.B. Gonzales, and E. Gouaux. 2007. Structure of acid-sensing ion channel 1 at 1.9 Å resolution and low pH. *Nature.* 449:316–323. http://dx.doi.org/10.1038/nature06163

Johnson, M.B., K. Jin, M. Minami, D. Chen, and R.P. Simon. 2001. Global ischemia induces expression of acid-sensing ion channel 2a in rat brain. *J. Cereb. Blood Flow Metab.* 21:734–740. http://dx.doi.org/10.1097/00004647-200106000-00011

Krishtal, O. 2003. The ASICs: Signaling molecules? Modulators? *Trends Neurosci.* 26:477–483. http://dx.doi.org/10.1016/S0166-2236(03)00210-8

Labarca, P., S.A. Simon, and R.R. Anholt. 1988. Activation by odorants of a multistate cation channel from olfactory cilia. *Proc. Natl. Acad. Sci. USA.* 85:944–947. http://dx.doi.org/10.1073/pnas.85.3.944

Li, M., E. Kratzer, K. Inoue, R.P. Simon, and Z.G. Xiong. 2010. Developmental change in the electrophysiological and pharmacological properties of acid-sensing ion channels in CNS neurons. *J. Physiol.* 588:3883–3900. http://dx.doi.org/10.1113/jphysiol.2010.192922

Lin, W., T. Ogura, and S.C. Kinnamon. 2002. Acid-activated cation currents in rat vallate taste receptor cells. *J. Neurophysiol.* 88:133–141.

Linster, C., M. Maloney, M. Patil, and M.E. Hasselmo. 2003. Enhanced cholinergic suppression of previously strengthened synapses enables the formation of self-organized representations in olfactory cortex. *Neurobiol. Learn. Mem.* 80:302–314. http://dx.doi.org/10.1016/S1074-7427(03)00078-9

Lledo, P.M., M. Alonso, and M.S. Grubb. 2006. Adult neurogenesis and functional plasticity in neuronal circuits. *Nat. Rev. Neurosci.* 7:179–193. http://dx.doi.org/10.1038/nrn1867

Mandairon, N., C. Stack, C. Kiselycznyk, and C. Linster. 2006. Broad activation of the olfactory bulb produces long-lasting changes in odor perception. *Proc. Natl. Acad. Sci. USA.* 103:13543–13548. http://dx.doi.org/10.1073/pnas.0602750103

Meng, Q.Y., W. Wang, X.N. Chen, T.L. Xu, and J.N. Zhou. 2009. Distribution of acid-sensing ion channel 3 in the rat hypothalamus. *Neuroscience.* 159:1126–1134. http://dx.doi.org/10.1016/j.neuroscience.2009.01.069

Miesenböck, G., D.A. De Angelis, and J.E. Rothman. 1998. Visualizing secretion and synaptic transmission with pH-sensitive green fluorescent proteins. *Nature.* 394:192–195. http://dx.doi.org/10.1038/28190

Mori, K. 1987. Membrane and synaptic properties of identified neurons in the olfactory bulb. *Prog. Neurobiol.* 29:275–320. http://dx.doi.org/10.1016/0301-0082(87)90024-4

Neale, J.H., T. Bzdega, and B. Wroblewska. 2000. *N*-Acetylaspartylglutamate: The most abundant peptide neurotransmitter in the mammalian central nervous system. *J. Neurochem.* 75:443–452. http://dx.doi.org/10.1046/j.1471-4159.2000.0750443.x

Pignataro, G., O. Cuomo, E. Esposito, R. Sirabella, G. Di Renzo, and L. Annunziato. 2011. ASIC1a contributes to neuroprotection elicited by ischemic preconditioning and postconditioning. *Int. J. Physiol. Pathophysiol. Pharmacol.* 3:1–8.

Ponsen, M.M., D. Stoffers, J. Booij, B.L. van Eck-Smit, E.Ch. Wolters, and H.W. Berendse. 2004. Idiopathic hyposmia as a preclinical sign of Parkinson's disease. *Ann. Neurol.* 56:173–181. http://dx.doi.org/10.1002/ana.20160

Price, M.P., G.R. Lewin, S.L. McIlwrath, C. Cheng, J. Xie, P.A. Heppenstall, C.L. Stucky, A.G. Mannsfeldt, T.J. Brennan, H.A. Drummond, et al. 2000. The mammalian sodium channel BNC1 is required for normal touch sensation. *Nature.* 407:1007–1011. http://dx.doi.org/10.1038/35039512

Price, M.P., S.L. McIlwrath, J. Xie, C. Cheng, J. Qiao, D.E. Tarr, K.A. Sluka, T.J. Brennan, G.R. Lewin, and M.J. Welsh. 2001. The DRASIC cation channel contributes to the detection of cutaneous touch and acid stimuli in mice. *Neuron.* 32:1071–1083. http://dx.doi.org/10.1016/S0896-6273(01)00547-5

Shepherd, G.M. 1972. Synaptic organization of the mammalian olfactory bulb. *Physiol. Rev.* 52:864–917.

Sherwood, T.W., and C.C. Askwith. 2009. Dynorphin opioid peptides enhance acid-sensing ion channel 1a activity and acidosis-induced neuronal death. *J. Neurosci.* 29:14371–14380. http://dx.doi.org/10.1523/JNEUROSCI.2186-09.2009

Sherwood, T.W., K.G. Lee, M.G. Gormley, and C.C. Askwith. 2011. Heteromeric acid-sensing ion channels (ASICs) composed of ASIC2b and ASIC1a display novel channel properties and contribute to acidosis-induced neuronal death. *J. Neurosci.* 31:9723–9734. http://dx.doi.org/10.1523/JNEUROSCI.1665-11.2011

Sherwood, T.W., E.N. Frey, and C.C. Askwith. 2012. Structure and activity of the acid-sensing ion channels. *Am. J. Physiol. Cell Physiol.* 303:C699–C710. http://dx.doi.org/10.1152/ajpcell.00188.2012

Shors, T.J., G. Miesegaes, A. Beylin, M. Zhao, T. Rydel, and E. Gould. 2001. Neurogenesis in the adult is involved in the formation of trace memories. *Nature.* 410:372–376. http://dx.doi.org/10.1038/35066584

Trombley, P.Q., and G.M. Shepherd. 1993. Synaptic transmission and modulation in the olfactory bulb. *Curr. Opin. Neurobiol.* 3:540–547. http://dx.doi.org/10.1016/0959-4388(93)90053-2

Trombley, P.Q., and G.L. Westbrook. 1990. Excitatory synaptic transmission in cultures of rat olfactory bulb. *J. Neurophysiol.* 64:598–606.

Usrey, W.M. 2002. AMPA autoreceptors fill the gap in olfactory temporal coding. *Nat. Neurosci.* 5:1108–1109. http://dx.doi.org/10.1038/nn1102-1108

Vodyanoy, V., and R.B. Murphy. 1983. Single-channel fluctuations in bimolecular lipid membranes induced by rat olfactory epithelial homogenates. *Science.* 220:717–719. http://dx.doi.org/10.1126/science.6301014

Waldmann, R., and M. Lazdunski. 1998. H^+-gated cation channels: neuronal acid sensors in the NaC/DEG family of ion channels. *Curr. Opin. Neurobiol.* 8:418–424. http://dx.doi.org/10.1016/S0959-4388(98)80070-6

Waldmann, R., F. Bassilana, J. de Weille, G. Champigny, C. Heurteaux, and M. Lazdunski. 1997a. Molecular cloning of a non-inactivating proton-gated Na^+ channel specific for sensory neurons. *J. Biol. Chem.* 272:20975–20978. http://dx.doi.org/10.1074/jbc.272.34.20975

Waldmann, R., G. Champigny, F. Bassilana, C. Heurteaux, and M. Lazdunski. 1997b. A proton-gated cation channel involved in acid-sensing. *Nature.* 386:173–177. http://dx.doi.org/10.1038/386173a0

Waldmann, R., G. Champigny, E. Lingueglia, J.R. De Weille, C. Heurteaux, and M. Lazdunski. 1999. H^+-gated cation channels. *Ann. NY Acad. Sci.* 868:67–76. http://dx.doi.org/10.1111/j.1749-6632.1999.tb11274.x

Wang, W.Z., X.P. Chu, M.H. Li, J. Seeds, R.P. Simon, and Z.G. Xiong. 2006. Modulation of acid-sensing ion channel currents, acid-induced increase of intracellular Ca^{2+}, and acidosis-mediated neuronal injury by intracellular pH. *J. Biol. Chem.* 281:29369–29378. http://dx.doi.org/10.1074/jbc.M605122200

Wemmie, J.A., J. Chen, C.C. Askwith, A.M. Hruska-Hageman, M.P. Price, B.C. Nolan, P.G. Yoder, E. Lamani, T. Hoshi, J.H. Freeman Jr., and M.J. Welsh. 2002. The acid-activated ion channel ASIC contributes to synaptic plasticity, learning, and memory. *Neuron.* 34:463–477. http://dx.doi.org/10.1016/S0896-6273(02)00661-X

Wemmie, J.A., C.C. Askwith, E. Lamani, M.D. Cassell, J.H. Freeman Jr., and M.J. Welsh. 2003. Acid-sensing ion channel 1 is localized in brain regions with high synaptic density and contributes to fear conditioning. *J. Neurosci.* 23:5496–5502.

Wemmie, J.A., M.P. Price, and M.J. Welsh. 2006. Acid-sensing ion channels: advances, questions and therapeutic opportunities. *Trends Neurosci.* 29:578–586. http://dx.doi.org/10.1016/j.tins.2006.06.014

Weng, J.Y., Y.C. Lin, and C.C. Lien. 2010. Cell type-specific expression of acid-sensing ion channels in hippocampal interneurons. *J. Neurosci.* 30:6548–6558. http://dx.doi.org/10.1523/JNEUROSCI.0582-10.2010

Westenhoefer, J. 2005. Age and gender dependent profile of food choice. *Forum Nutr.* 57:44–51. http://dx.doi.org/10.1159/000083753

Wilson, R.S., S.E. Arnold, Y. Tang, and D.A. Bennett. 2006. Odor identification and decline in different cognitive domains in old age. *Neuroepidemiology.* 26:61–67. http://dx.doi.org/10.1159/000090250

Wilson, R.S., J.A. Schneider, S.E. Arnold, Y. Tang, P.A. Boyle, and D.A. Bennett. 2007. Olfactory identification and incidence of mild cognitive impairment in older age. *Arch. Gen. Psychiatry.* 64:802–808. http://dx.doi.org/10.1001/archpsyc.64.7.802

Wu, L.J., B. Duan, Y.D. Mei, J. Gao, J.G. Chen, M. Zhuo, L. Xu, M. Wu, and T.L. Xu. 2004. Characterization of acid-sensing ion channels in dorsal horn neurons of rat spinal cord. *J. Biol. Chem.* 279:43716–43724. http://dx.doi.org/10.1074/jbc.M403557200

Wu, P.Y., Y.Y. Huang, C.C. Chen, T.T. Hsu, Y.C. Lin, J.Y. Weng, T.C. Chien, I.H. Cheng, and C.C. Lien. 2013. Acid-sensing ion channel-1a is not required for normal hippocampal LTP and spatial memory. *J. Neurosci.* 33:1828–1832. http://dx.doi.org/10.1523/JNEUROSCI.4132-12.2013

Xiong, Z.G., K.A. Pelkey, W.Y. Lu, Y.M. Lu, J.C. Roder, J.F. MacDonald, and M.W. Salter. 1999. Src potentiation of NMDA receptors in hippocampal and spinal neurons is not mediated by reducing zinc inhibition. *J. Neurosci.* 19:RC37.

Xiong, Z.G., X.M. Zhu, X.P. Chu, M. Minami, J. Hey, W.L. Wei, J.F. MacDonald, J.A. Wemmie, M.P. Price, M.J. Welsh, and R.P. Simon. 2004. Neuroprotection in ischemia: Blocking calcium-permeable acid-sensing ion channels. *Cell.* 118:687–698. http://dx.doi.org/10.1016/j.cell.2004.08.026

Xiong, Z.G., X.P. Chu, and R.P. Simon. 2007. Acid sensing ion channels—novel therapeutic targets for ischemic brain injury. *Front. Biosci.* 12:1376–1386. http://dx.doi.org/10.2741/2154

Zha, X.M., J.A. Wemmie, S.H. Green, and M.J. Welsh. 2006. Acid-sensing ion channel 1a is a postsynaptic proton receptor that affects the density of dendritic spines. *Proc. Natl. Acad. Sci. USA.* 103:16556–16561. http://dx.doi.org/10.1073/pnas.0608018103